Analysis of Deformations of the Tunnel Excavation Face via Simplified Calculation Methods

applied sciences

MDPI

Article

Analysis of Deformations of the Tunnel Excavation Face via Simplified Calculation Methods

Alireza Kalantar and Pierpaolo Oreste *

Department of Environmental, Land and Infrastructure Engineering, Politecnico di Torino, 10129 Turin, Italy
* Correspondence: pierpaolo.oreste@polito.it

Abstract: The stability of the excavation face during the excavation of a tunnel is necessary to safeguard the lives of workers and to guarantee regular and rapid progress of the works. In this paper, the stability conditions of the tunnelling face were analysed using simplified numerical calculation methods (one-step approach) and analytical methods, in order to evaluate the extrusion of the tunnelling face as a representative quantity of the mechanical behaviour of the rock ahead of it. A comparison between the numerical method and the hemispherical method was illustrated, which was able to demonstrate how the latter can be used with high reliability in this type of study. An extensive parametric analysis of the typical conditions encountered in the excavation of tunnels in weak rock made it possible to determine the extent of the face extrusion and the effect on it of the main considered geometric and geomechanical parameters. Thanks to the comparison of the extrusion values obtained from the calculation with the limit value indicated by the scientific literature, it is possible to arrive at a rapid assessment on the stability of the face. A specific study on the role of the pressure applied to the face on the extent of the extrusion then made it possible to understand how to proceed to define the intensity of the main stabilisation systems (TBM thrust and longitudinal fiberglass bolts) to avoid the risk of collapse of the excavation face.

Keywords: tunnel face stability; face extrusion; stress–strain state; numerical modelling; analytical method

Citation: Kalantar, A.; Oreste, P. Analysis of Deformations of the Tunnel Excavation Face via Simplified Calculation Methods. *Appl. Sci.* **2023**, *13*, 12683. https://doi.org/10.3390/app132312683

Academic Editor: Tiago Miranda

Received: 28 October 2023
Revised: 20 November 2023
Accepted: 21 November 2023
Published: 26 November 2023

1. Introduction

Tunnel construction has played a vital role in the development of modern infrastructure, providing efficient transportation, and facilitating communication systems. However, the process of tunnel excavation is not without challenges, and one of the most significant problems is the instability of the excavation face during the tunnel excavation. Its stability is of utmost importance for the safety of the personnel and plants present inside the tunnel. This issue becomes even more critical as tunnel depths increase [1–5].

Numerous factors, such as hydrological conditions, construction procedures, and geological circumstances, can lead to excavation face instability. These elements may have an impact on the support structure's efficacy as well as the rock or soil mass's stability. There could be fatalities, serious harm to the tunnel's integrity, and delays in building if the excavation face collapses. Therefore, it is imperative to identify any potential instability in the excavation face prior to starting construction, particularly in deeper and more complex tunnels [1,6–9].

Accurately anticipating ground conditions and the complexity of the geology present a significant problem in evaluating excavation face stability. Numerous analytical techniques, like as observational methods, empirical approaches, and numerical models, have been developed to assess the stability of the excavation face. These techniques are not always precise, though, and occasionally, the excavation face may remain unstable even after the proper support measures have been put in place. Consequently, in order to handle excavation face stability difficulties during tunnel construction, a thorough risk management plan is needed [7].

The stability of the excavation face in shallow tunnels is affected by several factors such as soil type, overburden pressure, and groundwater level. Soft soils, such as clays and silts, are particularly prone to face instability due to their low strength and high compressibility. Additionally, the overburden pressure exerted by the soil above the excavation face can cause deformations and failure of the face [10]. In some cases, groundwater seepage can also contribute to the destabilization of the excavation face, particularly in regions with high water table levels [11]. To prevent or mitigate face instability in shallow tunnels, various measures can be adopted such as using reinforcement techniques and grouting. Reinforcement techniques such as fibreglass dowels and shotcrete can be used to stabilize the excavation face and prevent its collapse. It is also possible to improve the strength and stability of the soil around an ahead of an excavation face by grouting: in this procedure, cement-based grout is injected into the soil in order to fill voids and enhance shear strength [12].

Tunnel face instability can also be encountered during the construction of deep tunnels, i.e., tunnels where the depth of the tunnel axis is greater than 10–12 times its radius [13–16]. In modern tunnel construction, full-face excavation is becoming a popular method to improve the efficiency and effectiveness of the tunnelling process. By utilizing large-scale machinery and equipment, this approach aims to optimize the use of available resources and streamline the construction process. This method is being adopted in various scenarios to make tunnel excavation more systematic and efficient [17]. Experts have long recognized the advantages of full-face excavation, dating back at least a century, and have advocated its use wherever possible. This method is highly beneficial in improving the efficiency of the tunnel construction process and can lead to significant time and cost savings. Despite its age, the practice remains relevant and valuable in modern tunnel construction [18]. However, the stability of the tunnel face is a critical concern for ensuring tunnel stability in numerous circumstances [19]. The stability of the tunnel face can be influenced not only by geological factors, such as the presence of unstable ground or poor-quality soil that is prone to squeezing, but also by the effects of construction techniques and environmental conditions. This adds to the intricacy of studying and ensuring tunnel stability [20].

Previous experiences have demonstrated that the most crucial aspect of effective tunnel design and construction in such situations is the ability to thoroughly study the ground deformation response and accurately assess the ground's capacity to stabilize and sustain itself [21]. During the preliminary research stage, it is crucial for the designer to take into account not only the radial displacement of the tunnel wall, but also the extrusion deformation of the tunnel face, as illustrated in Figure 1. Experimental evidence suggests that the analysis of the extrusion behaviour of the "core" located ahead of the tunnel face is the most critical factor in the ground's deformation response, which in turn is necessary for ensuring continuous progress in full-face excavation [2]. Excavation of the rock mass in front of the tunnel face can cause disturbance and plastic damage within a specific range. If left unaddressed, this can lead to large-scale collapse. In these cases, it is crucial to implement specific pre-reinforcement measures for the advanced core of the tunnel face. Conservative protected intervention and conservative reinforcement intervention are two approaches that can be used to ensure the stability of the advance core and reduce extrusion deformation of the tunnel face. These measures involve applying face pressure using a full-face machine or a support structure at the face (conservative protected intervention) or realizing longitudinal fiberglass bolts (conservative reinforcement intervention) [22,23].

This work presents a simplified numerical approach to examine the tunnel face's stress and strain status and determine whether or not an intervention is necessary to stabilise the excavation face. An analytical method is used to compare the face extrusion values that were obtained via the numerical modelling.

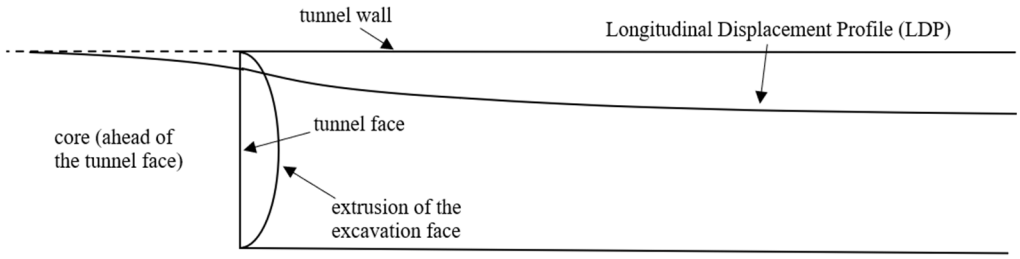

Figure 1. Ground deformation response during the full-face excavation on the tunnel face (extrusion) and the tunnel walls (radial displacements).

2. Stress and Strain Condition of the Tunnel Face via Hemispherical Approach

Using a hemisphere, whose radius matches that of the tunnel and is positioned as shown in Figure 2, one can assess for a deep tunnel, with a certain degree of accuracy, the stress and strain behaviour of the excavation face and of the ground ahead of it. This study can lead to the evaluation of the type of behaviour of the soil or rock: elastic or elasto-plastic [7]. When a plastic zone is detected in a cortical portion of the hemisphere, this usually means that the ground on the excavation face and for a certain distance from it is unstable to some extent. The level of instability depends on how thick the plastic zone is and on the residual strength parameters of the soil or rock, i.e., the strength parameters shown by the ground within the plastic zone, the area where the ground behaves in the plastic field. In these circumstances, the excavation face may collapse or experience the breaking of pieces of material into different sizes. By approximating the excavation face as a hemisphere, it becomes feasible to evaluate the radial and circumferential stresses and radial displacements using the spherical symmetry as a powerful calculation tool.

The mathematical treatment of the stress and strain behaviour of the ground around the spherical surface is reported in the paper [7]. In this work, steps are developed that allow the values of the stresses and strains in the material at the boundary of the spherical surface to be obtained, both in the elastic behaviour zone and in the plastic field.

Several hypotheses have been proposed for the convergence–confinement method, which is utilized for analysing stresses in the ground [3,24–26]. One such hypothesis assumes that the lithostatic stresses are homogenous and isotropic, i.e., the stresses in the medium before creating the hemispheric void are equal to P_0 in all directions. Based on this assumption, the radial stresses σ_r (which act radially toward the sphere center), the circumferential stresses σ_θ (oriented perpendicular to the radial direction), and the radial displacement ur in the ground around a sphere can be described under elastic behaviour conditions by simple equations [7]:

$$\sigma_\theta = P_0 + 0.5 \cdot (P_0 - p) \cdot \frac{R^3}{r^3} \quad (1)$$

$$\sigma_r = P_0 - (P_0 - p) \cdot \frac{R^3}{r^3} \quad (2)$$

$$u_r = \frac{1+\nu}{2 \cdot E} \cdot (P_0 - p) \cdot \frac{R^3}{r^2} \quad (3)$$

where the following are defined:
P_0: the lithostatic stress that exists at a tunnel depth;
R: the sphere radius;
r: the distance from the sphere centre ($r \geq R$);
p: the radial pressure applied to the tunnel face (on the inner surface of the hemisphere);
E, n: the elastic modulus and Poisson's ratio of the ground.

On the surface of the hemisphere ($r = R$), the following value of the radial displacement u_R is obtained [7]:

$$u_R = \frac{1+\nu}{2 \cdot E} \cdot (P_0 - p) \cdot R \quad (4)$$

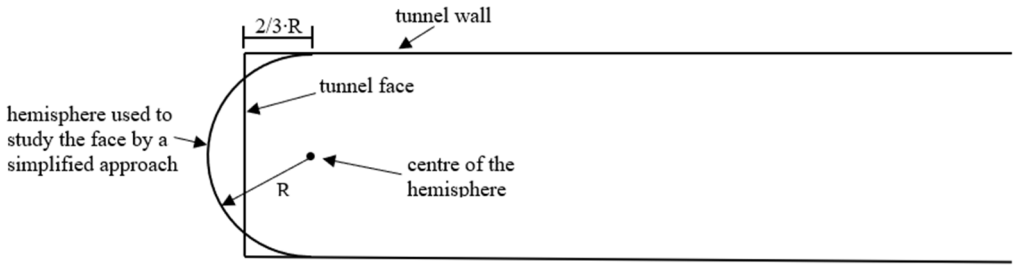

Figure 2. The excavation face modelled using a hemisphere with a radius equivalent to the tunnel one. The hemisphere's centre is shifted a distance 2/3 that of the tunnel radius behind the excavation face. Key: R is the tunnel radius.

If a plastic zone exists around the hemisphere, with an extension from R to the plastic radius R_{pl}, the material within this zone is considered to exhibit a plastic behaviour. Beyond the plastic zone (i.e., for $r > R_{pl}$), the material is assumed to behave elastically, and the radial and circumferential stresses can be calculated using the following equations [7]:

$$\sigma_\theta = P_0 + 0.5\left(P_0 - \sigma_{Rpl}\right)\frac{{R_{pl}}^3}{r^3} \tag{5}$$

$$\sigma_r = P_0 - \left(P_0 - \sigma_{Rpl}\right)\frac{{R_{pl}}^3}{r^3} \tag{6}$$

where the following are defined:

R_{pl}: the plastic radius, i.e., the maximum distance from the centre of the plastic zone:

$$R_{pl} = R \cdot \left[\frac{\left[\frac{3}{2}\cdot P_0 \cdot \left(1 - sen\phi_p\right) - 2\cdot c_p \cdot cos\phi_p\right]\cdot tg\phi_r}{\left(\frac{3}{2} + \frac{1}{2}\cdot sen\phi_p\right)\cdot c_r} + 1\right]^{\frac{1}{2\cdot(N_\Phi^r - 1)}} \tag{7}$$

σ_{Rpl}: the radial stress at the plastic radius R_{pl}:

$$\sigma_{Rpl} = \frac{\frac{3}{2}\cdot P_0 \cdot \left(1 - sen\phi_p\right) - 2\cdot c_p \cdot cos\phi_p}{\left(\frac{3}{2} + \frac{1}{2}\cdot sen\phi_p\right)} \tag{8}$$

c_p and ϕ_p: the peak cohesion and friction angle of the ground;
c_r and ϕ_r: the residual cohesion and friction angle of the ground.

In the presence of a zone with a plastic behaviour, the radial displacement u_R of the surface of the hemisphere, for the zero pressure p case, is given by the following expression [7]:

$$\begin{aligned} u_R(r = R; p = 0) = \frac{1}{E}\cdot\Bigg[&\frac{1+\nu}{2}\cdot\frac{R_{pl}^{2\cdot N_\Psi+1}}{R^{2\cdot N_\Psi}}\cdot\frac{\left(P_0 + \frac{c_p}{tg\phi_p}\right)\cdot sen\phi_p}{\left(\frac{3}{4} + \frac{1}{4}\cdot sen\phi_p\right)} + \frac{(1 - 4\cdot\nu\cdot N_\Psi + 2\cdot N_\Psi - 2\cdot\nu)}{2\cdot N_\Psi + 1}\cdot\left(P_0 + \frac{c_r}{tg\phi_r}\right)\cdot \\ &\left(\frac{R_{pl}^{2\cdot N_\Psi+1}}{R^{2\cdot N_\Psi}} - R\right) - \frac{[1 - 2\cdot\nu\cdot N_\Psi + 2\cdot N_\Phi^r\cdot(N_\Psi - \nu\cdot N_\Psi - \nu)]}{[2\cdot(N_\Phi^r + N_\Psi) - 1]\cdot R^{(2\cdot N_\Phi^r - 1)}}\cdot\left(\frac{c_r}{tg\phi_r}\right)\cdot\left(\frac{R_{pl}^{2\cdot(N_\Phi^r+N_\Psi)-1}}{R^{2\cdot N_\Psi}} - R^{2\cdot N_\Phi^r - 1}\right)\Bigg] \end{aligned} \tag{9}$$

where the following are defined:

$$N_\Psi = \frac{1 + sen\psi}{1 - sen\psi}$$

Ψ: the dilatancy angle, the angle able to describe the plastic deformations development in the plastic zone.

$$N_\phi^r = \frac{1 + sen\phi_r}{1 - sen\phi_r}$$

Thanks to Equation (4) (for the elastic case, when σ_{Rpl} in Equation (8) is lower than or equal to 0) and 9 (for the elastic-plastic case, when σ_{Rpl} in Equation (8) is higher than 0) it is possible to obtain the radial displacement of the hemisphere in the specific site conditions; it appears to be a good estimation of the extrusion displacement that occurs at the excavation face.

3. Axisymmetric Numerical Modelling of the Excavation Face

A detailed numerical model was developed using the two-dimensional explicit finite difference code FLAC2D 8.1 in the axisymmetric configuration. The model was used to analyse the stress and strain conditions in the ground during the construction phases of a circular tunnel supported by a concrete lining. An homogeneous and hydrostatic stress state was assumed, where the initial state of stress was kept constant in the model regardless of the direction.

The boundary conditions of the model involve the application of an in situ stress equal to P_0 on all borders, except on the axis of axial symmetry of the tunnel (y axis in Figure 3).

The following further assumptions were made:

The chosen criterion for the ground failure is the Mohr–Coulomb one, which is commonly used for weaker rocks that exhibit less curvature in their strength criterium.
The post-failure behaviour of the rock was assumed to be ideal elastic-plastic, with residual strength parameters equal to the peak ones.
The elastic modulus was assumed to be constant in both the elastic and plastic phases.
The dilatancy angle, denoted as ψ, was assumed to be zero (the minimum value that can be reached). This means that the strain behaviour in the plastic zone is characterized by constant volume plastic strains, following the approach described by [27–29] for deep rocks with weak mechanical properties.
The concrete lining was assumed to have a constant elastic modulus of 30,000 MPa and Poisson's ratio of 0.15, which are typical values for concrete materials.

A parametric analysis was developed considering three types of weak rocks, where problems regarding the stability of the excavation face can be encountered: rock with poor mechanical properties (Type A), medium mechanical properties (Type B), and good mechanical properties (Type C).

Type A had a cohesion ($c_p = c_r$) of 0.3 MPa, friction angle ($\Phi_p = \Phi_r$) of 25°, and an elastic modulus E of 4000 MPa.
Type B with a cohesion ($c_p = c_r$) of 0.9 MPa, friction angle ($\Phi_p = \Phi_r$) of 30°, and an elastic modulus E of 8000 MPa.
Type C with a cohesion ($c_p = c_r$) of 1.5 MPa, friction angle ($\Phi_p = \Phi_r$) of 35°, and an elastic modulus E of 12,000 MPa.

The Poisson's ratio was considered 0.3 for all three studied rock types.

A total of 27 numerical models were developed for each rock type, considering different combinations obtained by changing the following geometrical parameters:

Tunnel radius, R (2, 3.5, and 5 m);
Thickness of the concrete lining (0.1, 0.2, and 0.3 m);
In situ vertical stress (P_0) (1.1, 5.5, and 11 MPa).

The purpose of this analysis was to analyse as many instances as possible of those that may occur during the construction of medium-to-large diameter horizontal tunnels in weak rock formations at different depths from the surface.

Figure 3 illustrates the scheme of the developed axisymmetric numerical model: the bottom and top of the model are constrained in the Y direction and the in situ pressure is applied on the right side. The tunnel axis coincides with the Y axis, and also, only one half of the tunnel and of the surrounding ground is simulated in the model thanks to the symmetry of the problem. The simulation of the tunnel advancement and the lining construction starts on the top of the model towards its centre, where the stress and strain state is analysed.

The size of the model varies with the radius of the simulated tunnel: in the radial direction, it goes from 65 m (case of tunnel with radius 2m) to 163 m (tunnel with radius 5 m); in the longitudinal one from 100 m (radius 2 m) to 250 m (radius 5 m).

The number of quadrilateral elements used to simulate the excavated zone is 10. Quadrilateral elements are also adopted to represent both the concrete lining and the rock surrounding the tunnel. The total number of quadrilateral elements used for each considered geometry is shown in Table 1.

Table 1. Geometrical characteristics of the numerical model, varying the tunnel radius.

Radius	In the X Direction	In the Y Direction	Total Number of Quadrilateral Elements
2.0 m	65	100	6500
3.5 m	115	176	20,240
5.0 m	163	250	40,750

Each of the numerical models foresaw simulations of both excavation steps (each advancing step with a length of 1.2 m along the tunnel axis) and support installation, in order to be able to reproduce as faithfully as possible the real conditions during the tunnel construction: 17 advancement steps were implemented. The simulation began at the top border of the model and continued until it reached the centre. The excavation was simulated by simply removing elements in the tunnel area, while the support installation was considered by reactivating elements in the zone occupied by the support structure, attributing the mechanical properties of concrete. These elements were deemed to be in an initial state of zero stress when reactivated.

For each studied case, the stresses and strains within the model were evaluated (in Figures 4 and 5, there is an example of the obtained results, with reference to the case of a tunnel with a radius of 2 m, lining thickness of 20 cm, in situ stress of 11 MPa, excavated in a Good Rock (type C).

Another simplified numerical model was adopted in the study, maintaining the same geometries and rock types considered for the detailed model. The simplified model adopts a quick single-step simulation instead of a step-by-step approach. In the simplified model, the values of the rock elastic modulus E was varied (from the original value to 1/2, 1/3, 1/4, and 1/5 of it) so as to be able to verify whether an artificial modification of the rock stiffness is necessary in case one wishes to adopt simplified numerical modelling which does not reproduce the exact succession of the construction phases. After the analysis of the calculation results (Figures 6–8), it is clear that in the case of Good and Intermediate rock types, the face extrusion values obtained via the simplified model agree with those of the detailed model, maintaining the original value of the elastic modulus of the rock mass. However, in the context of poor mechanical properties (Type A of the rock mass), utilizing an elastic modulus of 1/5·E leads to face extrusion results of the simplified model better fitting those obtained from the calculation using the detailed model.

Thanks to the comparison developed on the calculation results, it is therefore possible to state that the simplified axisymmetric model (one step approach) is able to analyze the mechanical and deformation behaviour of the excavation face in order to evaluate its stability conditions.

From the conducted analyses, it was possible to detect how the simplified numerical modelling (one step approach) is able to correctly represent the deformation conditions of the excavation face in deep tunnels excavated in weak rocks, with the sole precaution of applying an artificial reduction in the elastic modulus of the rock mass at 1/5 of its real value, only when the mechanical characteristics are poor (i.e., type A of the rock mass).

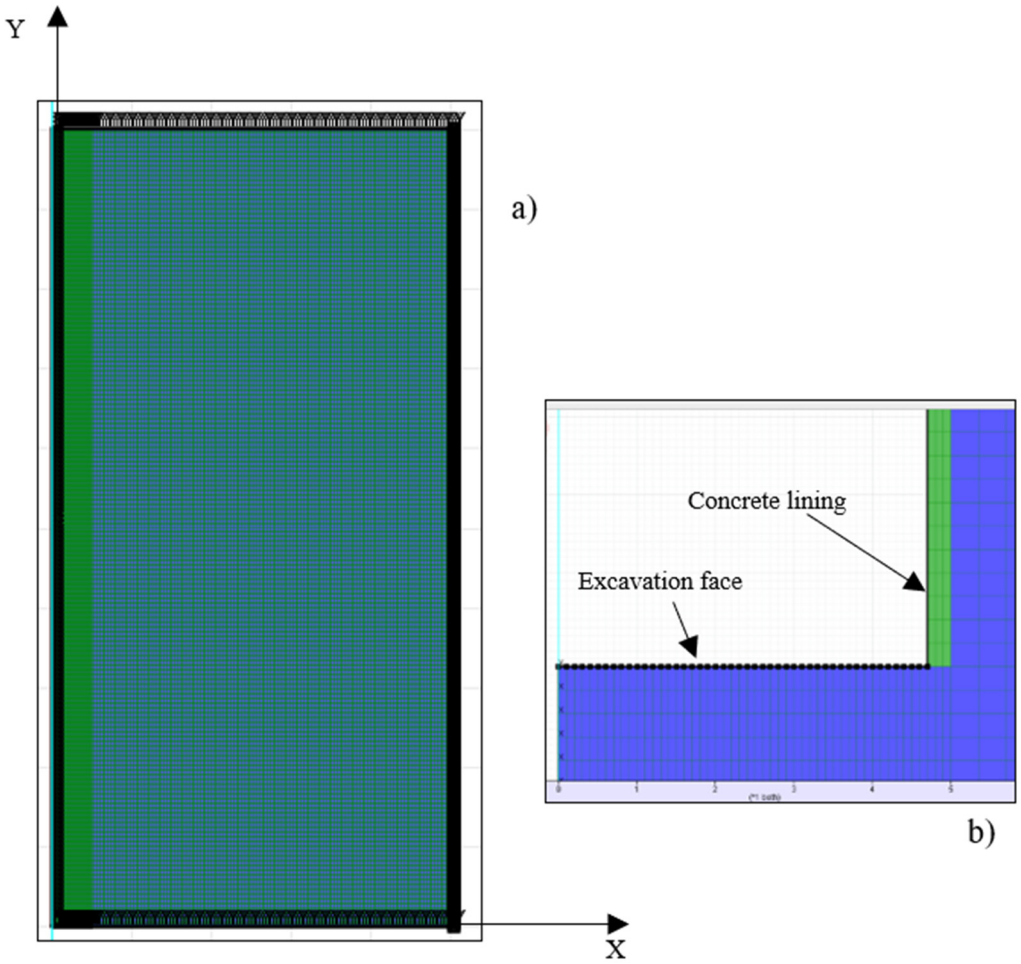

Figure 3. (**a**) Scheme of the whole developed axisymmetric numerical model to simulate the tunnel excavation (the green zone is the area of the tunnel, the blue zone the rock mass surrounding the tunnel); (**b**) Detail of the mesh of the model close to the excavation face (the green zone refers to the 3 elements used to simulate the concrete lining).

4. Reliability of the Hemispherical Approach

After conducting 81 numerical simulations with the simplified model, significant and valuable results have been obtained on the deformation of the excavation face. These findings are illustrated in the accompanying figures, which provide visual representations of the outcomes. It was possible also to compare the obtained results with those from analytical methods (hemispherical approach). In this particular case, the extrusion at the centre of the face obtained from the numerical calculation is compared with the radial inward displacement of the sphere (Figures 9–11).

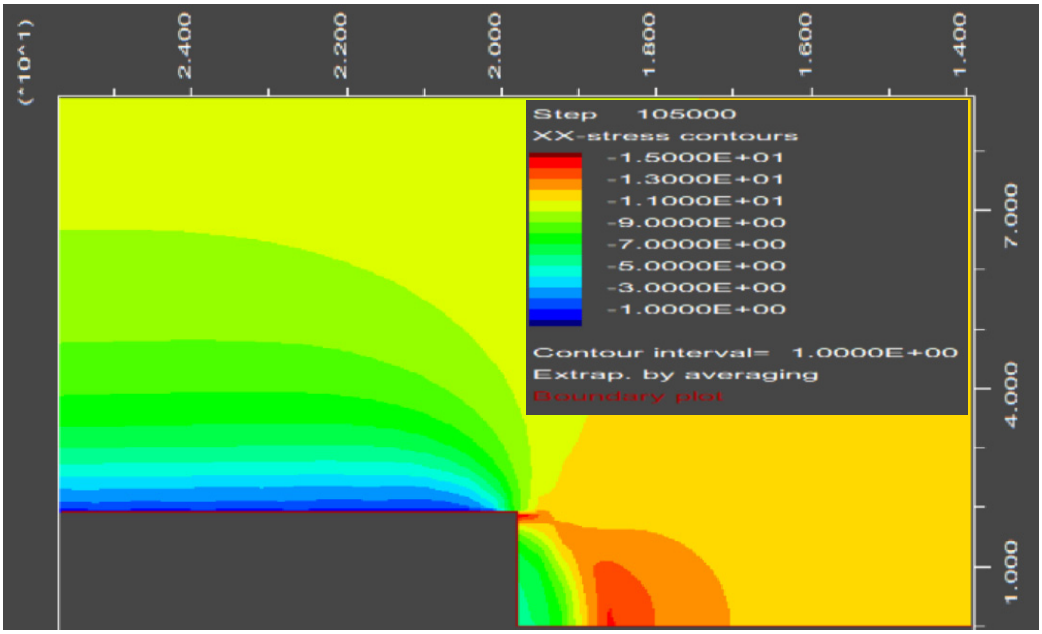

Figure 4. Vertical stresses in the rock (in front of the excavation face and at the contour of the excavated profile), for the case of a tunnel with a radius of 2 m, thickness of the lining 20 cm, P_0 = 11 MPa, excavated in a Good rock mass (type C).

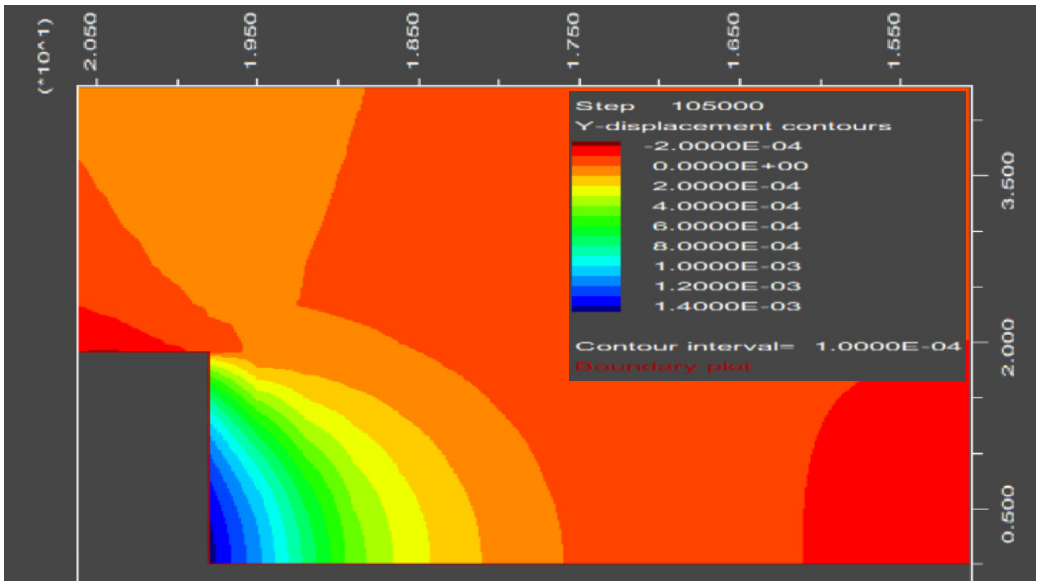

Figure 5. Horizontal displacements (extrusion) in the rock ahead of the excavation face, for the case of a tunnel with a radius of 2 m, thickness of the lining 20 cm, P_0 = 11 MPa, excavated in a Good rock mass (type C).

The comparison between the simulated extrusion values and the ones obtained from the spherical method facilitates a quantitative evaluation of the simulation's accuracy. If the results align closely, it provides confidence in the simulation model's ability to accurately represent the behaviour of the studied phenomenon. By incorporating this validation step, the researchers can ensure that the simulation results are trustworthy and can be used with confidence for further analysis and decision-making. It helps to establish the credibility and reliability of the simulation approach employed in the study. The comparison is performed for tunnels with radii of 2, 3.5, and 5 m with different values of lining thickness and in situ stress state, respectively.

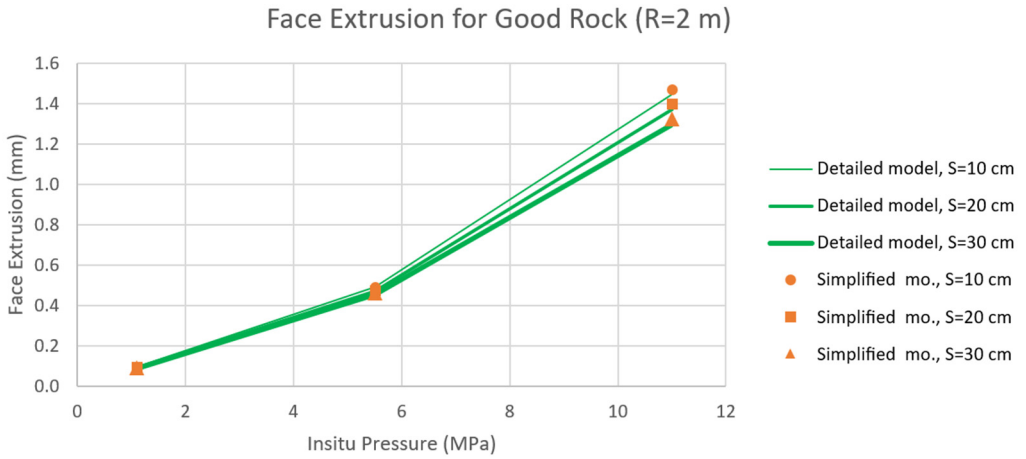

Figure 6. Comparison of the Tunnel Face Extrusion in Good rock (type C): Detailed Numerical Model vs. Simplified Numerical Models (with the original E value), varying the Lining Thickness S (10, 20, 30 cm).

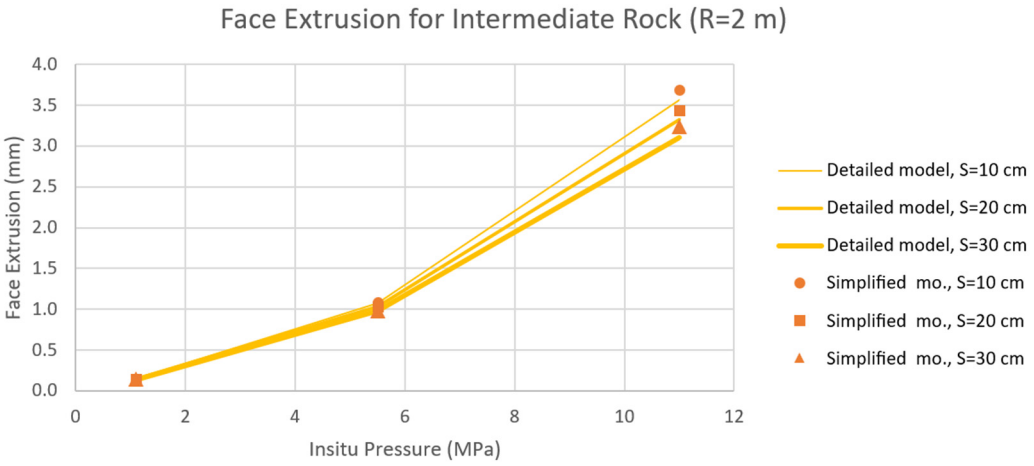

Figure 7. Comparison of the tunnel face extrusion in Intermediate rock (type B): detailed numerical model vs. simplified numerical models (with the original E value), varying the lining thickness S (10, 20, 30 cm).

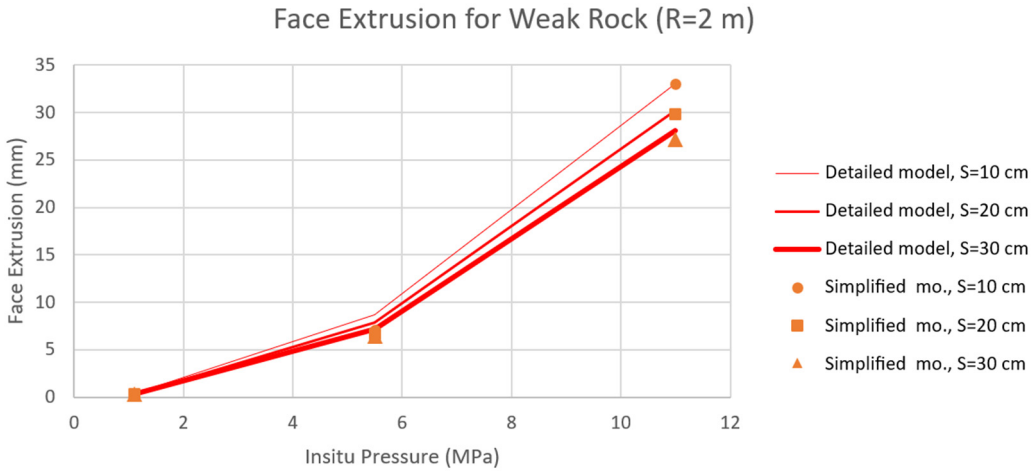

Figure 8. Comparison of the tunnel face extrusion in Poor rock (type A): detailed numerical model vs. simplified numerical models (with the decreased value of the elastic modulus 1/5·E), varying the lining thickness S (10, 20, 30 cm).

The spherical method, which does not take into account the thickness of the lining, provides a single value for face extrusion. In contrast, the simulation results consider different lining thicknesses. It is worth noting that the face extrusion values obtained from the spherical method closely align with the average extrusion values observed for linings with thicknesses of 10, 20, and 30 cm. It is important to note that the results presented in this section pertain to a specific scenario where the face pressure is assumed to be zero. The purpose of this simulation was to replicate a mechanized excavation process, where the face pressure is not a significant factor.

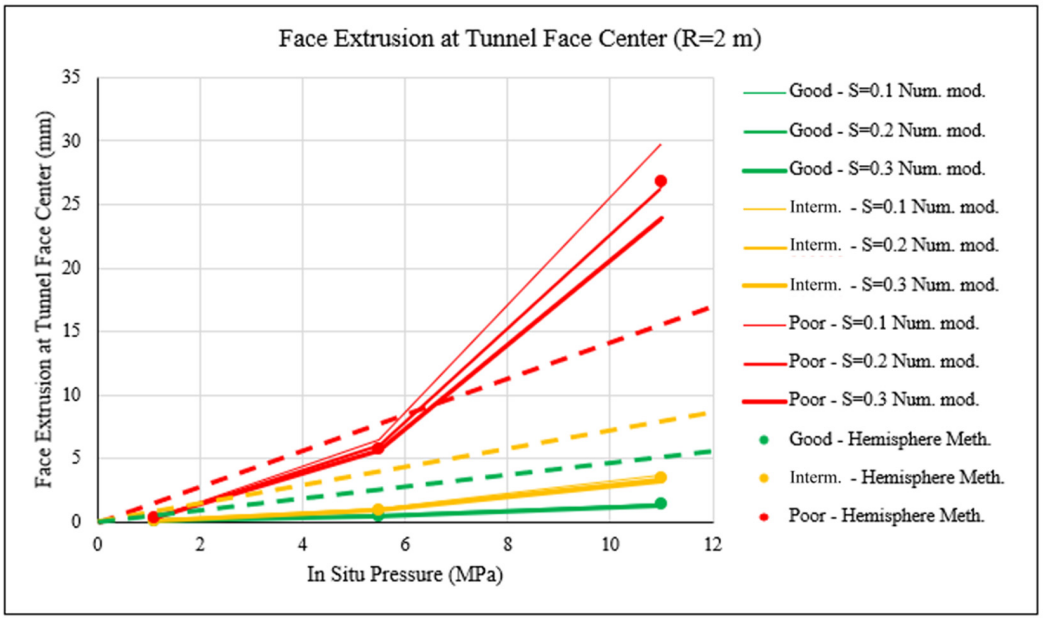

Figure 9. Face extrusion at the centre of the tunnel face: simplified numerical modelling and hemispherical approach (R = 2 m). Key: S: the concrete lining thickness; Good: rock mass type C; Intermediate: type B; Poor: type A; dashed lines: maximum admissible extrusion values for type C (green), type B (yellow), and type A (red), according to [30].

From the analysis of the figures, it is possible to note how the type of rock and the in situ stress have an important effect on the extent of extrusion of the excavation face. More specifically, for a P_0 of 11 MPa (corresponding to a tunnel depth of 425–475 m) and poor characteristics of the rock mass (type A), a clear increase in extrusion is seen, denoting an intense plasticization of the of excavation face. This aspect is detectable for all three analysed tunnel radii. As regards the influence of the thickness of the concrete lining, it is appreciable only in the case of a very deep tunnel (P_0 = 11 MPa) and rock mass with poor mechanical characteristics: in this case, a variability of approximately 10% of the extrusion can be detected as a function of the thickness of the lining (the variability increases to 15% for a tunnel with a small radius (R = 2 m). In all other cases, the influence of the thickness (and, therefore, of the stiffness) of the lining on the extrusion of the excavation face is to be considered negligible.

Furthermore, as can be seen from the same Figures 9–11, the estimate of the extrusion obtained from the simplified hemispherical method is in line with the results obtained from the numerical modelling, for each analysed case; for the case of a deep tunnel (P_0 = 11 MPa) and Poor rock (type A) the result of the simplified hemispherical method is intermediate to the variability range of the extrusion due to the different thickness of the concrete lining.

Georgiou et al. [30] analysed the stability of the excavation faces of deep tunnels through three-dimensional numerical modelling. After an extensive parametric analysis, by varying the main geometric parameters of the tunnel (two tunnel sizes, three tunnel depths) and geomechanical parameters of the rock mass (two horizontal thrust coefficients K_0 and

four sets of material parameters), they were able to obtain the dimensionless trend of the face extrusion parameter Ω_f as the dimensionless face stability parameter Λ_f varies [30]:

$$\Omega_f = 1.4 \cdot \Lambda_f^{-1.2} \tag{10}$$

where the following are defined:

$$\Omega_f = \left(\frac{u_h}{2 \cdot R}\right) \cdot \left(\frac{E}{P_0}\right)$$

u_h: face extrusion (horizontal displacement);

$$\Lambda_f = 3.8 \cdot \left(\frac{\sigma_{cm}}{P_0 \cdot \sqrt{1 + \frac{2}{3} \cdot K_0}}\right) \cdot \left(\frac{P_0}{2 \cdot \gamma \cdot R}\right)^{0.35}$$

σ_{cm}: rock mass uniaxial strength:

$$\sigma_{cm} = \frac{2 \cdot c_p \cdot cos\Phi_p}{1 - sin\Phi_p}$$

γ: rock mass specific weight.

According to the authors [30], when Λ_f is equal to 1, the rate of increase in the face extrusion parameter Ω_f increases considerably, indicating the approach to a limit condition of stability. $\Lambda_f = 1$, therefore representing a limit condition for stability. Setting $\Lambda_f = 1$ in Equation (10), the maximum admissible extrusion to guarantee the stability conditions of the excavation face becomes [30]:

$$u_{h,lim} = \frac{2.8 \cdot P_0 \cdot R}{E} \tag{11}$$

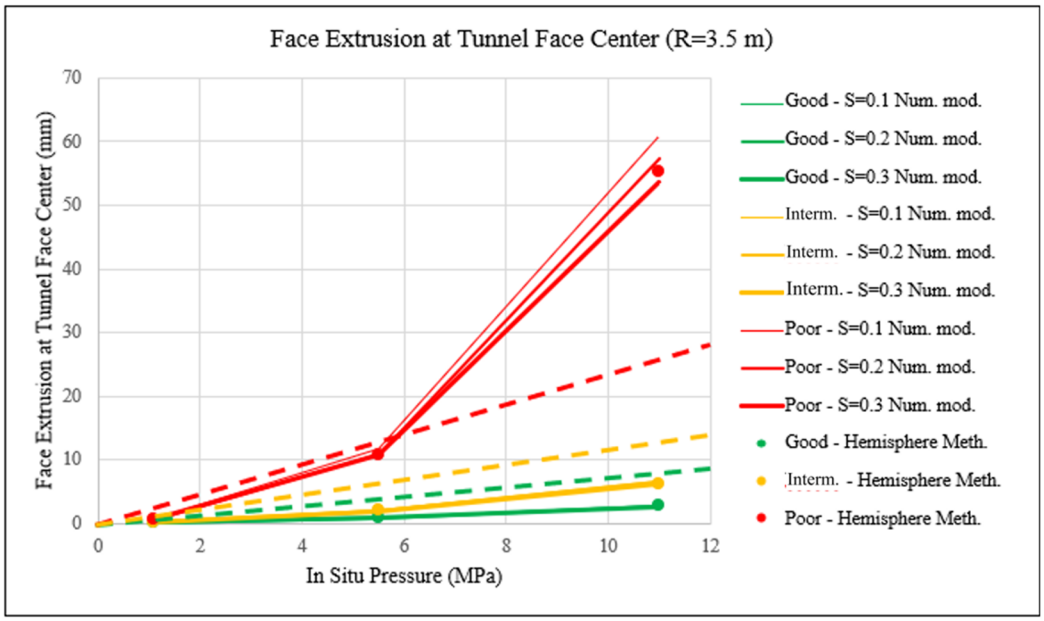

Figure 10. Face extrusion at the centre of the tunnel face: simplified numerical modelling and hemispherical approach (R = 3.5 m). Key: S: the concrete lining thickness; Good: rock mass type C; Intermediate: type B; Poor: type A; dashed lines: maximum admissible extrusion values for type C (green), type B (yellow), and type A (red), according to [30].

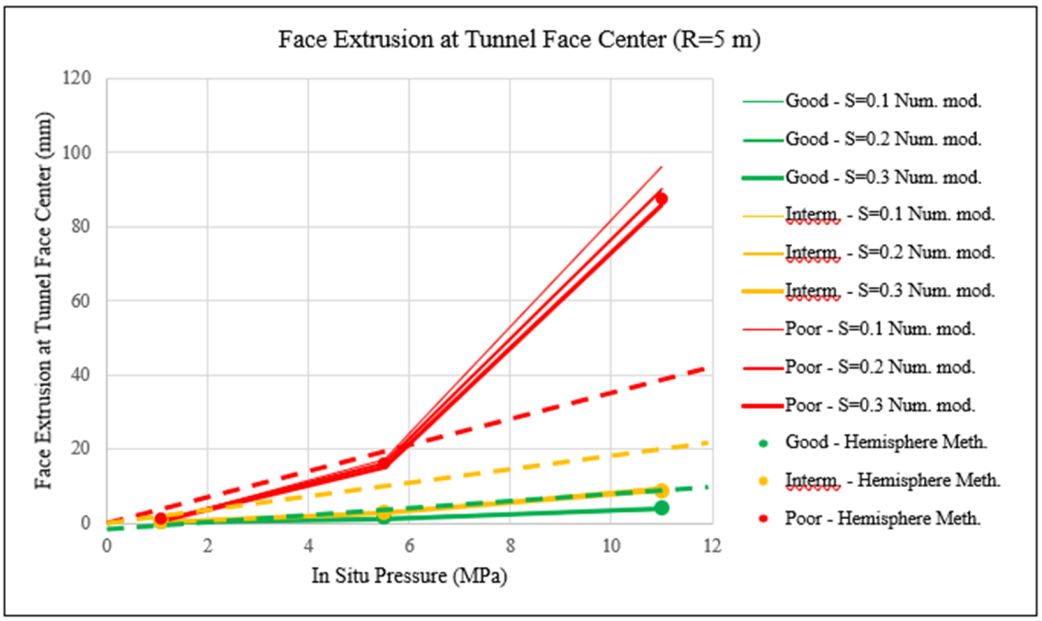

Figure 11. Face extrusion at the centre of the tunnel face: simplified numerical modelling and hemispherical approach (R = 5 m). Key: S: the concrete lining thickness; Good: rock mass type C; Intermediate: type B; Poor: type A; dashed lines: maximum admissible extrusion values for type C (green), type B (yellow), and type A (red), according to [30].

In Figures 9–11, these limit extrusion values are represented with dashed lines, with the colours referring to the considered different types of rock (types A, B, and C). Extrusions that are higher than the limit values denote potential conditions of instability of the excavation face. For the analysed cases, these conditions are detected only for rocks of type A, for in situ stresses higher than 5.8–6.2 MPa, depending on the tunnel size. The limit extrusions, however, are not reached for type B and C rocks, not even for the maximum in situ stress values adopted in the study (P_0 = 11 MPa).

The definition of a maximum horizontal displacement (Equation (11)) allows the stability of the face to be evaluated through monitoring systems, duly positioned on it, and capable of continuously evaluating the induced deformations [31]. The monitoring must be used considering the possible measurement errors and the precision that can be provided by the instruments used. To make the measurements more representative, the average value obtained from similar deformation measurements can be used [32–35].

5. The Effect of a Pressure Applied to the Excavation Face

The study also investigated the phenomenon of face extrusion during the tunnel construction under different face pressures. The analysis focused on evaluating the extent of face extrusion for various combinations of rock type, tunnel radius, lining thickness, and in situ stress state. The findings provide valuable insights into the effects of face pressure on the stabilization of the tunnel face. Figures 12–14 depict the impact of tunnel face pressures on the extrusion behaviour of a tunnel with a radius of 2 m, for the three values of the in situ stress from 1.1 to 11 MPa. From the figures, it can be seen how as the pressure applied to the excavation face increases, the extrusion is considerably reduced following a hyperbolic trend. Furthermore, the application of the pressure at the face is able to induce an extrusion that is lower than the limit one, permitting the stabilization of the tunnel face. From a design point of view, therefore, it can be very useful to identify the pressure at the face which is able to reduce the extrusion to values lower than the limit ones, thus allowing the elimination of the risk of instability of the excavation face during the tunnel excavation.

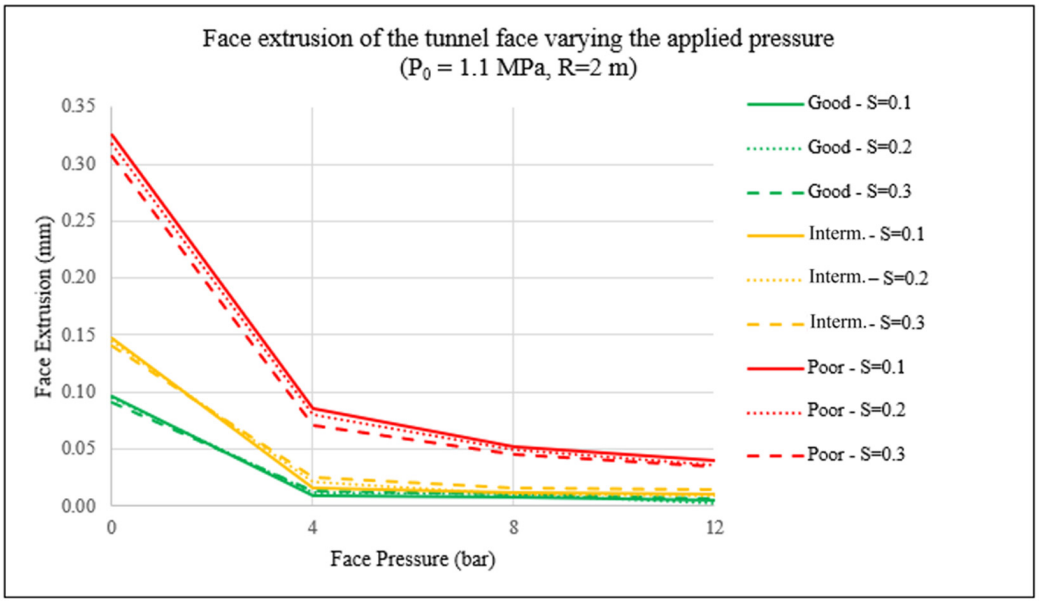

Figure 12. Face extrusion via the simplified numerical model, varying the pressure applied to the tunnel face. Case of R = 2 and P_0 = 1.1 MPa. Key: S: concrete lining thickness; Good: rock type C; Intermediate: type B; Poor: type A; $u_{h,lim}$ = 1.54 mm (type A), 0.77 mm (type B), and 0.51 mm (type C), according to [30].

Figures 15–17 provide a visual representation of the influence of tunnel face pressures on the extrusion behaviour of a tunnel with a larger radius of 3.5 m, and Figures 18–20 for a tunnel radius of 5 m. Furthermore, it is worth highlighting that the thickness of the lining has a minimal impact on the face extrusion, resulting in only a slight variation of its value only for the Poor type of rock. Another noteworthy outcome is that increasing the diameter of the tunnel a corresponding increase in the face extrusion can be seen.

In Figures 14, 17 and 20, the limit extrusion u_{hlim} was represented with a horizontal red dash dotted line. Through this representation, it is simple to identify the stabilization pressure to be applied to the face, in the case of Poor rock (type A), in order to obtain an extrusion lower than the limit one and, therefore, the guaranteed stability of the face during excavation. This pressure can simply be applied by the TBM head in the case of mechanized excavation; it is to be understood as an equivalent pressure that can also be provided by rock reinforcing (through longitudinal fiberglass bolts) in the case of excavation using the traditional advancing method.

The figures that have been obtained for this section allow the evaluation of the effect of the pressure applied to the excavation face on the level of rock deformation (extrusion). They therefore represent a useful design tool that can lead to the definition of the detailed characteristics of the TBM machine to be used in a specific case or in the definition of the number and dimensions of the fiberglass bolts that can be adopted to stabilize the excavation face of a tunnel.

6. Conclusions

Tunnel excavation face stability is a paramount concern, particularly in the construction of deep and complex tunnels, from a geological point of view. Key factors impacting tunnel face stability include rock strength, stress conditions, geological features, and support systems.

In this paper, the stability of the excavation face of deep tunnels in weak rocks was analysed through simplified numerical and analytical methods. More specifically, the extrusion (the horizontal movement) of the excavation face during the construction of the tunnel was studied. Different approaches of two-dimensional numerical modelling in the axisymmetric configuration were presented: a step-by-step approach with detailed

modelling of the excavation phases (advancement of the face) and installation of the supports; a simplified approach (one step) in which the tunnel is excavated all together, with the simultaneous installation of the support structures. Thanks to the comparison of the results, it was possible to verify that in some cases the simplified approach requires an artificial reduction in the elastic modulus of the rock in order to provide results on the face extrusion consistent with the detailed modelling (the step-by-step approach). The use of a simplified analytical method (the hemisphere method) [8] made it possible to detect how reliable and rigorous this method is in estimating the extrusion of the excavation face during the construction of the tunnel, guaranteeing fast calculation and an extensive investigation into the role of influencing parameters on the behaviour of the rock in that particular area of the tunnel.

This study presents an extensive parametric analysis in the typical variability fields of the main geometric and geomechanical parameters: from this study, it emerged that the mechanical characteristics of the rock play an important role in the deformation process of the face, together with the depth of the tunnel (i.e., the in situ state of stress); the stiffness of the support system has, however, a marginal role.

Thanks to the studies carried out by Georgiou et al. [33], it was then possible to compare the extrusions calculated with the illustrated numerical and analytical methods with the limit extrusion value associated with a potential instability of the excavation face. This comparison allows the verification of whether a specific tunnel requires a stabilizing intervention on the excavation face or not.

Finally, the role of a stabilizing intervention on the excavation face simulated through pressure applied to it was analysed via the proposed simplified numerical modelling (one-step approach). More specifically, it was possible to detect the reduction in extrusion with the increase in the applied pressure. Thanks to the identification of the limit extrusion value [28], it is therefore possible to proceed with a rapid evaluation of the intensity of the stabilization intervention (pressure applied by a tunnel boring machine or a rock reinforcement intervention through longitudinal fiberglass bolts) so as to bring the extrusion value to values lower than it.

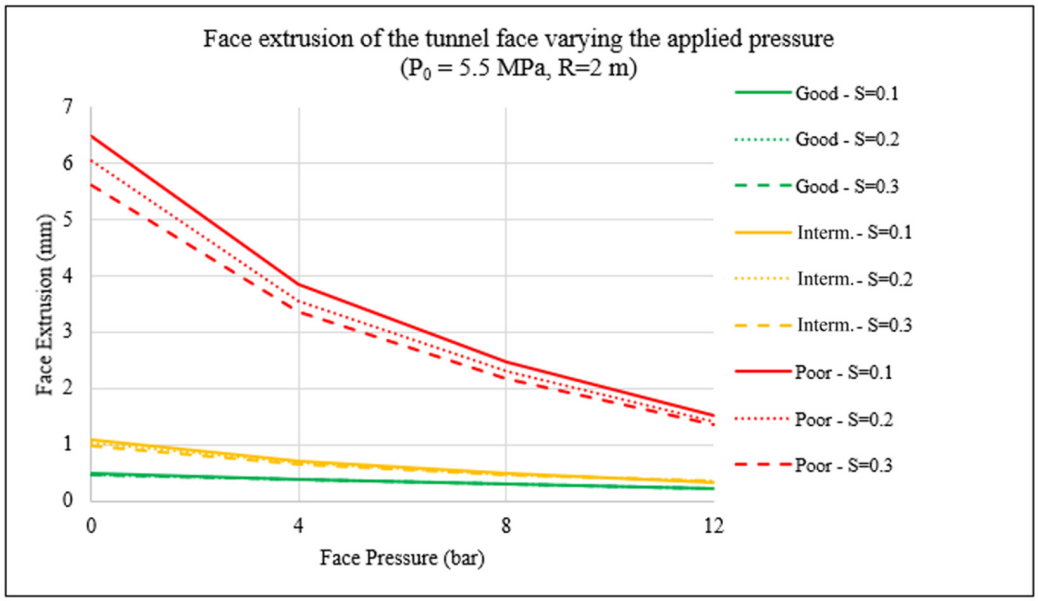

Figure 13. Face extrusion via the simplified numerical model, varying the pressure applied to the tunnel face. Case of R = 2 and P_0 = 5.5 MPa. Key: S: concrete lining thickness; Good: rock type C; Intermediate: type B; Poor: type A; $u_{h,lim}$ = 7.70 mm (type A), 3.85 mm (type B), and 2.57 mm (type C), according to [30].

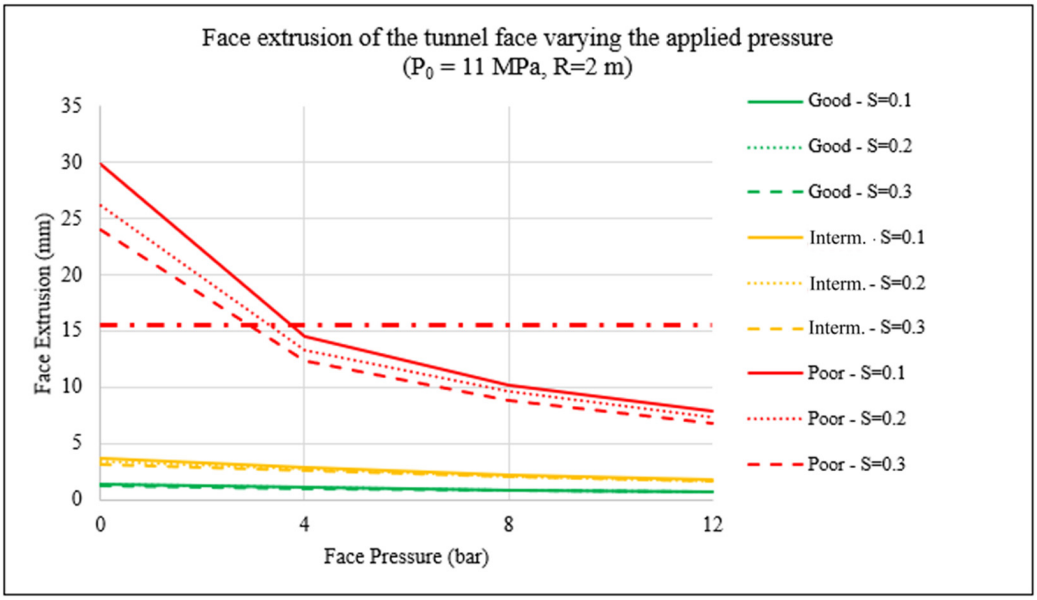

Figure 14. Face extrusion via the simplified numerical model, varying the pressure applied to the tunnel face. Case of R = 2 and P_0 = 11 MPa. Key: S: concrete lining thickness; Good: rock type C; Intermediate: type B; Poor: type A; $u_{h,lim}$ = 15.40 mm (type A), 7.70 mm (type B), and 5.13 mm (type C), according to [30]; the red dash dotted line represents the limit extrusion for the poor rock.

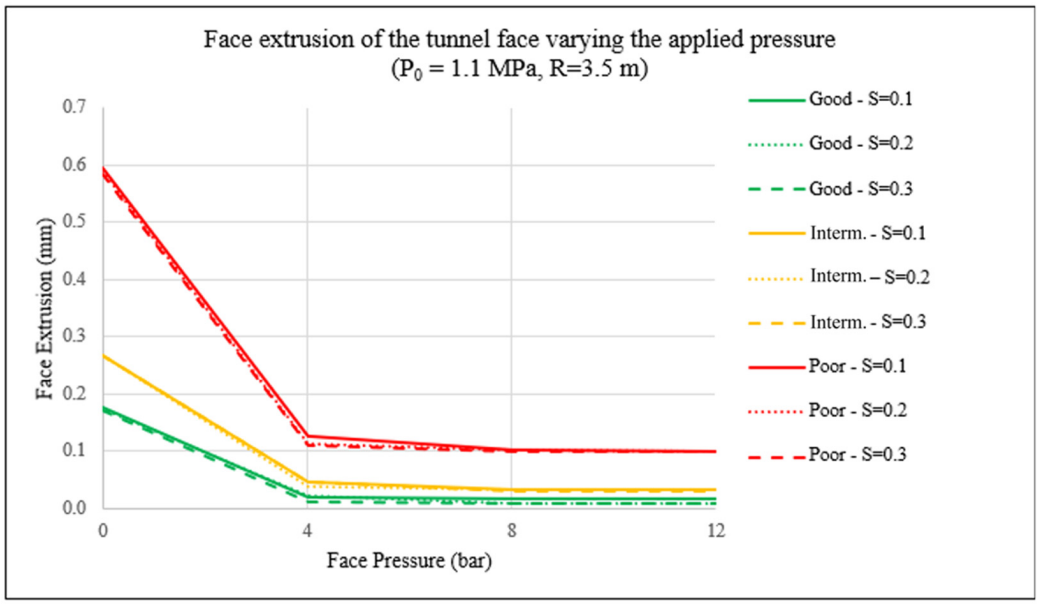

Figure 15. Face extrusion via the simplified numerical model, varying the pressure applied to the tunnel face. Case of R = 3.5 and P_0 = 1.1 MPa. Key: S: concrete lining thickness; Good: rock type C; Intermediate: type B; Poor: type A; $u_{h,lim}$ = 2.70 mm (type A), 1.35 mm (type B), and 0.90 mm (type C), according to [30].

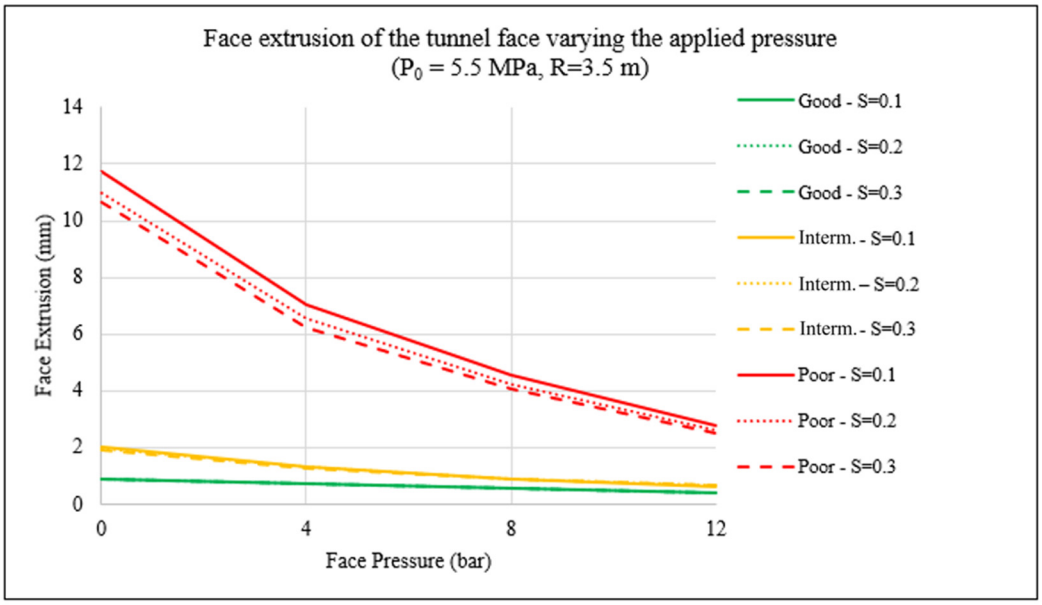

Figure 16. Face extrusion via the simplified numerical model, varying the pressure applied to the tunnel face. Case of R = 3.5 and P_0 = 5.5 MPa. Key: S: concrete lining thickness; Good: rock type C; Intermediate: type B; Poor: type A; $u_{h,lim}$ = 13.48 mm (type A), 6.74 mm (type B), and 4.49 mm (type C), according to [30].

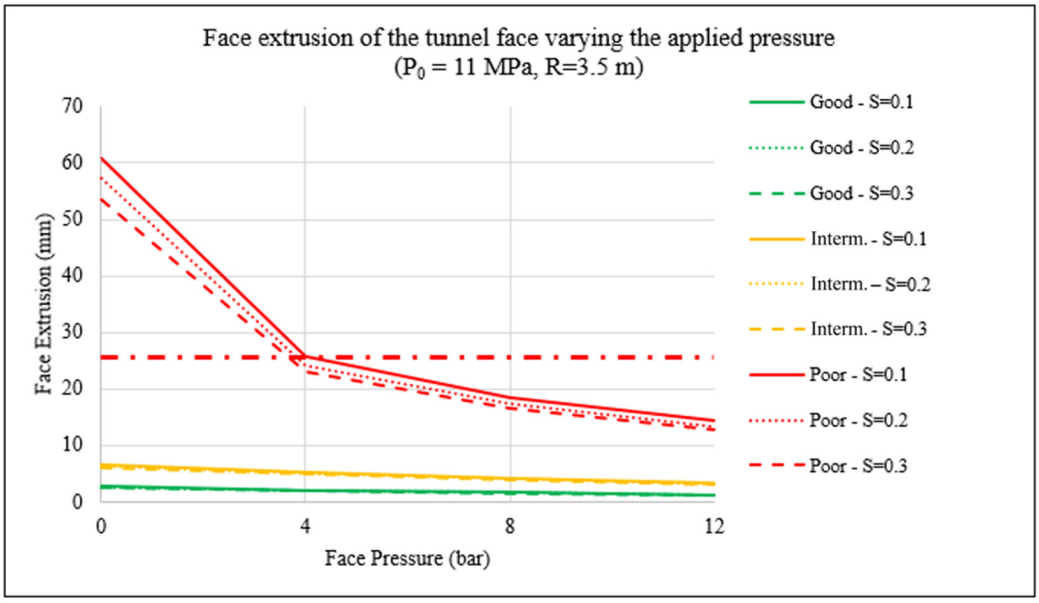

Figure 17. Face extrusion via the simplified numerical model, varying the pressure applied to the tunnel face. Case of R = 3.5 and P_0 = 11 MPa. Key: S: concrete lining thickness; Good: rock type C; Intermediate: type B; Poor: type A; $u_{h,lim}$ = 26.95 mm (type A), 13.48 mm (type B), and 8.98 mm (type C), according to [30]; the red dash dotted line represents the limit extrusion for the poor rock.

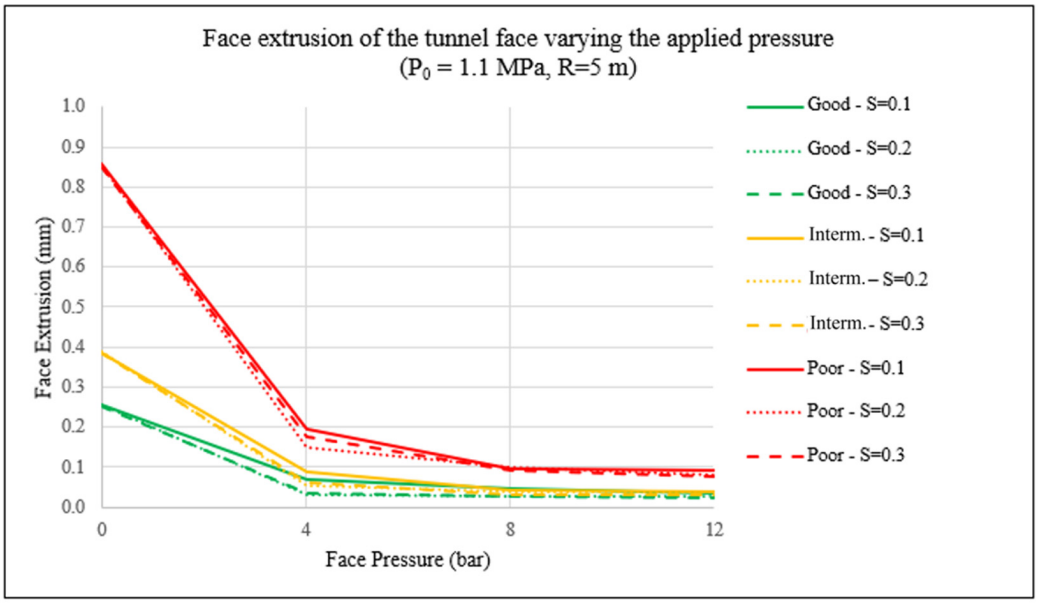

Figure 18. Face extrusion via the simplified numerical model, varying the pressure applied to the tunnel face. Case of R = 5 and P_0 = 1.1 MPa. Key: S: concrete lining thickness; Good: rock type C; Intermediate: type B; Poor: type A; $u_{h,lim}$ = 3.85 mm (type A), 1.93 mm (type B), and 1.28 mm (type C), according to [30].

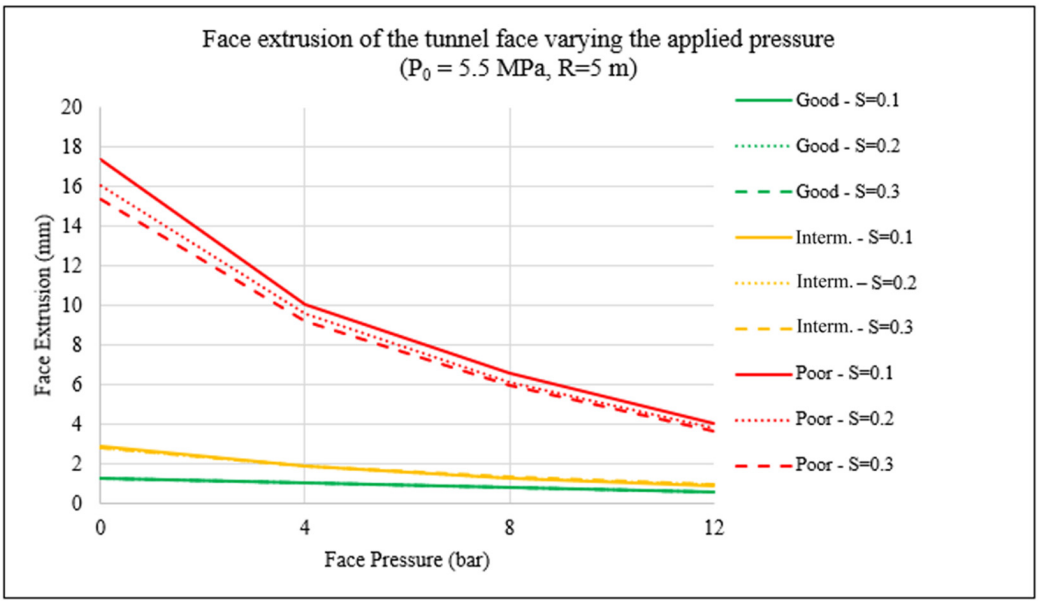

Figure 19. Face extrusion via the simplified numerical model, varying the pressure applied to the tunnel face. Case of R = 5 and P_0 = 5.5 MPa. Key: S: concrete lining thickness; Good: rock type C; Intermediate: type B; Poor: type A; $u_{h,lim}$ = 19.25 mm (type A), 9.63 mm (type B), and 6.42 mm (type C), according to [30].

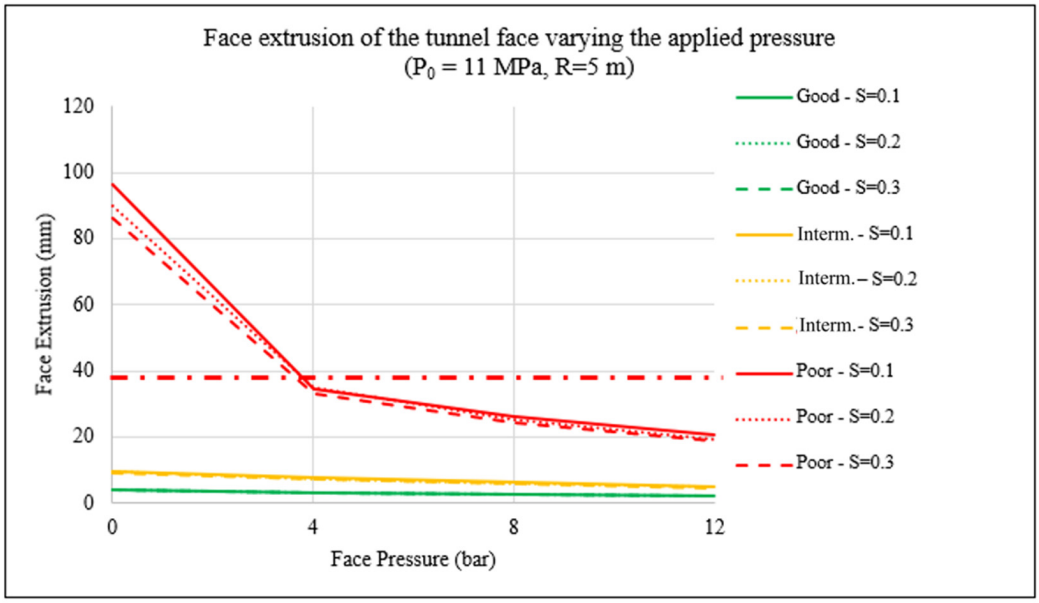

Figure 20. Face extrusion via the simplified numerical model, varying the pressure applied to the tunnel face. Case of R = 5 and P_0 = 11 MPa. Key: S: concrete lining thickness; Good: rock type C; Intermediate: type B; Poor: type A; $u_{h,lim}$ = 38.50 mm (type A), 19.25 mm (type B), and 12.83 mm (type C), according to [30]; the red dash dotted line represents the limit extrusion for the poor rock.

The proposed approach to the study of the problem of the stability of the excavation face in a deep tunnel and in particular to the analysis of the deformations of the rock ahead of it, while allowing quick analyses, appears to be reliable and, therefore, useful for the design phase of tunnels and other underground works, especially in the preliminary phase, when it is necessary to verify whether the excavation face in its natural condition presents risks of instability, or whether it is necessary to intervene with stabilization systems and with what intensity.

A future development of the research may concern the application of simplified calculation tools for the evaluation of the effects of fiberglass bolting on the stabilization of the tunnel excavation face.

Author Contributions: Conceptualization, P.O.; methodology, A.K. and P.O.; software, A.K. and P.O.; investigation, A.K. and P.O.; data curation, A.K.; writing—original draft preparation, A.K. and P.O.; writing—review and editing, A.K. and P.O.; supervision, P.O. All authors have read and agreed to the published version of the manuscript.

Funding: This research received no external funding.

Data Availability Statement: The data presented in this study are available on request from the corresponding author. The data are not publicly available due to large amount of dedicated memory.

Conflicts of Interest: The authors declare no conflict of interest.

References

1. Anagnostou, G.; Kovári, K. Face stability conditions with earth-pressure-balanced shields. *Tunn. Undergr. Space Technol.* **1996**, *11*, 165–173. [CrossRef]
2. Lunardi, P. *Design and Construction of Tunnels: Analysis of Controlled Deformation in Rocks and Soils (ADECO-RS)*; Springer Science & Business Media: Berlin/Heidelberg, Germany, 2008; pp. 1–576.
3. Oreste, P. Face stabilisation of shallow tunnels using fibreglass dowels. *Proc. Inst. Civ. Eng.-Geotech. Eng.* **2009**, *162*, 95–109. [CrossRef]
4. Hernández, Y.Z.; Farfán, A.D.; de Assis, A.P. Three-dimensional analysis of excavation face stability of shallow tunnels. *Tunn. Undergr. Space Technol.* **2019**, *92*, 103062. [CrossRef]
5. Liu, W.; Chen, E.J.; Yao, E.; Wang, Y.; Chen, Y. Reliability analysis of face stability for tunnel excavation in a dependent system. *Reliab. Eng. Syst. Saf.* **2021**, *206*, 107306. [CrossRef]

6. Oreste, P. The convergence-confinement method: Roles and limits in modern geomechanical tunnel design. *Am. J. Appl. Sci.* **2009**, *6*, 757. [CrossRef]
7. Oreste, P. Evaluation of the tunnel face stability through a ground stress analysis with a hemispherical geometry approximation. *Am. J. Appl. Sci.* **2014**, *11*, 1995–2003. [CrossRef]
8. Zou, J.F.; Qian, Z.H.; Xiang, X.H.; Chen, G.H. Face stability of a tunnel excavated in saturated nonhomogeneous soils. *Tunn. Undergr. Space Technol.* **2019**, *83*, 1–17. [CrossRef]
9. Eshraghi, A.; Zare, S. Face stability evaluation of a TBM-driven tunnel in heterogeneous soil using a probabilistic approach. *Int. J. Geomech.* **2015**, *15*, 04014095. [CrossRef]
10. Wang, L.; Chen, W.; Tan, X.; Tan, X.; Yang, J.; Yang, D.; Zhang, X. Numerical investigation on the stability of deforming fractured rocks using discrete fracture networks: A case study of underground excavation. *Bull. Eng. Geol. Environ.* **2020**, *79*, 133–151. [CrossRef]
11. Zhang, Z.; Li, H.; Yang, H.; Wang, B. Failure modes and face instability of shallow tunnels under soft grounds. *Int. J. Damage Mech.* **2019**, *28*, 566–589. [CrossRef]
12. Han, K.; Wang, X.; Hou, B.; Lin, X.; Cao, C.J. Analysis of Instability Mode and Limit Support Pressure of Shallow Tunnel Face in Sands. *Symmetry* **2020**, *12*, 2067. [CrossRef]
13. Boldini, D.; Graziani, A.; Ribacchi, R. Raticosa Tunnel, Italy: Characterization of Tectonized Clay-Shale and Analysis of Monitoring Data and Face Stability. *Soils Found.* **2004**, *44*, 57–69. [CrossRef]
14. Kamata, H.; Mashimo, H. Centrifuge model test of tunnel face reinforcement by bolting. *Tunn. Undergr. Space Technol.* **2003**, *18*, 205–212. [CrossRef]
15. Kirsch, A. Experimental investigation of the face stability of shallow tunnels in sand. *Acta Geotech.* **2010**, *5*, 43–62. [CrossRef]
16. Wong, H.; Subrin, D.; Dias, D. Extrusion movements of a tunnel head reinforced by finite length bolts—A closed-form solution using homogenization approach. *Int. J. Numer. Anal. Methods Geomech.* **2000**, *24*, 533–565. [CrossRef]
17. Tan, C.H. Solution of a bolted spherical cavity in elastoplastic medium and its application to extrusion analysis of tunnel face. *Rock Mech. Rock Eng.* **2020**, *53*, 3055–3072. [CrossRef]
18. Barla, G. Full-face excavation of large tunnels in difficult conditions. *J. Rock Mech. Geotech. Eng.* **2016**, *8*, 294–303. [CrossRef]
19. Oreste, P. Face stabilization of deep tunnels using longitudinal fibreglass dowels. *Int. J. Rock Mech. Min. Sci.* **2013**, *58*, 127–140. [CrossRef]
20. Chen, X.; He, P.; Yan, D.; Nie, A. Face Stability and Reinforcement of the Tunnel in Weak Surrounding Rock. *Geotech. Geol. Eng.* **2020**, *38*, 5511–5521. [CrossRef]
21. Lunardi, P.; Barla, G. Full face excavation in difficult ground. *Geomech. Tunn.* **2014**, *7*, 461–468. [CrossRef]
22. Paternesi, A.; Schweiger, H.F.; Scarpelli, G. Numerical analyses of stability and deformation behavior of reinforced and unreinforced tunnel faces. *Comput. Geotech.* **2017**, *88*, 256–266. [CrossRef]
23. Qian, Z.; Zou, J.; Pan, Q.; Dias, D.J. Safety factor calculations of a tunnel face reinforced with umbrella pipes: A comparison analysis. *Eng. Struct.* **2019**, *199*, 109639. [CrossRef]
24. Berthoz, N.; Branque, D.; Subrin, D.; Wong, H.; Humbert, E. Face failure in homogeneous and stratified soft ground: Theoretical and experimental approaches on 1g EPBS reduced scale model. *Tunn. Undergr. Space Technol.* **2012**, *30*, 25–37. [CrossRef]
25. Osgoui, R.; Oreste, P. Convergence-control approach for rock tunnels reinforced by grouted bolts, using the homogenization concept. *Geotech. Geol. Eng.* **2007**, *25*, 431–440. [CrossRef]
26. Osgoui, R.R.; Oreste, P. Elasto-plastic analytical model for the design of grouted bolts in a Hoek–Brown medium. *Int. J. Numer. Anal. Methods Geomech.* **2010**, *34*, 1651–1686. [CrossRef]
27. Hoek, E.; Brown, E.T. Practical estimates of rock mass strength. *Int. J. Rock Mech. Min. Sci.* **1997**, *34*, 1165–1186. [CrossRef]
28. Alejano, L.R.; Alonso, E. Considerations of the dilatancy angle in rocks and rock masses. *Int. J. Rock Mech. Min. Sci.* **2005**, *42*, 481–507. [CrossRef]
29. Alejano, L.R.; Rodriguez-Dono, A.; Alonso, E.; Manín, G.F. Ground reaction curves for tunnels excavated in different quality rock masses showing several types of post-failure behaviour. *Tunn. Undergr. Space Technol.* **2009**, *24*, 689–705. [CrossRef]
30. Georgiou, D.; Kalos, A.; Kavvadas, M. 3D Numerical Investigation of Face Stability in Tunnels With Unsupported Face. *Geotech. Geol. Eng.* **2022**, *40*, 355–366. [CrossRef]
31. Yang, C.; Xia, Y. Interval Pareto front-based multi-objective robust optimization for sensor placement in structural modal identification. *Reliab. Eng. Syst. Saf.* **2024**, *242*, 109703. [CrossRef]
32. Yang, C.; Lu, W.; Xia, Y. Uncertain optimal attitude control for space power satellite based on interval Riccati equation with non-probabilistic time-dependent reliability. *Aerosp. Sci. Technol.* **2023**, *139*, 108406. [CrossRef]
33. Yang, C.; Lu, W.; Xia, Y. Positioning accuracy analysis of industrial robots based on non-probabilistic time-dependent reliability. *IEEE Trans. Reliab.* **2023**, 1–14. [CrossRef]
34. Sharafat, A.; Tanoli, W.A.; Raptis, G.; Seo, J.W. Controlled blasting in underground construction: A case study of a tunnel plug demolition in the Neelum Jhelum hydroelectric project. *Tunn. Undergr. Space Technol.* **2019**, *93*, 103098. [CrossRef]
35. Sharafat, A.; Khan, M.S.; Latif, K.; Seo, J. BIM-based tunnel information modeling framework for visualization, management, and simulation of drill-and-blast tunneling projects. *J. Comput. Civ. Eng.* **2021**, *35*, 04020068. [CrossRef]